Research Article

SOHAG JOURNAL OF SCIENCES

https://doi.org/10.21608/sjsci.2024.255448.1164

Investigating the Effects of Ag and Zn Metals as Pre-coating with Annealing on Physical Properties and Applications of MnS Thin Films

H. A. Mohamed[1], E. Kh. Shokr[1], M. F. Hasaneen[2,3], A. A. Ismail[1,*], H. M. Ali[1]

[1] *Physics Department, Faculty of Science, Sohag University, 82524 Sohag, Egypt*
[2] *Physics Department, College of Science, Jouf University, Al-Jouf, Sakaka, P.O. Box 2014, Sakaka, Saudi Arabi*
[3] *Thin Films and Nanotechnology Lab, Physics Department, Faculty of Science, Sohag University, 82524, Sohag, Egypt*
[*] *Email: a.ali.sci1106@gmail.com*

Received: 14th December 2023, **Revised:** 11th February 2024, **Accepted:** 20th February 2024
Published online: 20th March 2024

Abstract: For this study, we used thermal evaporation to synthesize thin films of manganese sulfide (MnS) with a layer of zinc and silver pre-coating. A range of methods, including UV/VIS/NIR spectrophotometry, EDX, X-ray diffraction (XRD), field emission scanning electron microscopy (FE-SEM), and the two-probe technique, were employed to examine the structural, morphological, optical, and electrical characteristics of the as-deposited and annealed films. Additionally, the films were annealed for 20 min at 300°C. Numerous parameters were found, including the dispersion parameters, activation energy, mobility, refractive index, extinction coefficient, Urbach energy, dielectric constants, and optical energy gap. The pure MnS, metal/MnS, and annealed metal/MnS films had an amorphous structure. There was a direct allowed transition between the films with different pre-coating layers. The energy gaps were 3.17 eV for MnS, 2.57 eV for Ag/MnS, 2.52 eV for Zn/MnS, 1.9 eV for annealed Ag/MnS, and 2.6 eV for annealed Zn/MnS. Besides, the pre-coating layer affected the refractive index dispersion of the films. In addition, the addition of the pre-coating metal resulted in lower film resistivity, indicating semiconductor behavior in the samples. Finally, we tested deposited and annealed Ag/MnS films for sensing I_2 and Co_2. As a result, deposited Ag/MnS has a promising future for gas sensing applications. In addition, we tested annealed Zn/MnS for organic pollutant decomposition, which demonstrated high efficiency of approximately 81%.
Keywords: Thin-film MnS; pre-coating metal layer; gas sensing, photocatalysis.

1. Introduction

Manganese sulfides (MnS_x) have gained significant attention due to their special qualities and possible uses in solar cells, optoelectronic, and luminous devices, photocatalysis, and gas sensing applications **[1].** These compounds are abundant in the Earth's crust, making them an appealing material for various technological advancements. MnS exists in different phases, as well as α-, β-, and γ-MnS. Elevated temperatures or pressures can convert the metastable phases β-MnS and γ-MnS into α-MnS [2-4]. Scientists have employed a variety of methods, including chemical vapor deposition [5], thermal evaporation [6], solvothermal synthesis [7], and radio frequency sputtering, to create MnS thin films with varying morphologies. **[8]**. The choice of preparation technique significantly influences the properties of thin films. Thermal evaporation is an affordable, simple, and convenient method for depositing broad-area thin films on a variety of substrates. The addition of MnS to the surface of glass with a pre-applied metal layer can improve its electrical and optical properties **[9].**

For gas sensing and photocatalytic applications, the impact of the annealing procedure and the pre-coating layer of Ag and Zn metals on the structural, optical, and electrical properties of MnS thin films has been investigated in the current work. Zn/MnS thin films that are both pure and metal-precoated have been deposited using the thermal evaporation process. We examined the structural, morphological, optical, and electrical characteristics of the produced films using X-ray diffraction (XRD), scanning electron microscopy (SEM), energy-dispersive X-ray spectroscopy (EDX), UV/VIS/NIR spectrophotometry, and the two-probe approach. We tested the formed films as photocatalysts for water purification, specifically for degrading organic pollutants like methyl blue (MB). In addition, for gas sensor applications, the pure MnS films and Ag pre-coating films were analyzed concerning their exposure to I_2 and CO_2 gases.

2. Experimental

Using a specialized coating apparatus (E306A, made under license from Edwards Ltd.), pure MnS and Ag and Zn pre-coated layers with a thickness of 10 nm and a total film thickness of 300 nm were deposited by a thermal evaporation technique. Cold-pressed MnS powder tablets with 99.999% purity were put in a tungsten boat that had a high melting point of 3422°C for the deposition operation. A molybdenum boat with a melting point of 2650°C was employed to deposit the metal layer. These crushed MnS tablets and bulk metals were placed onto meticulously cleaned micron-sized glass surfaces. The substrates were cleaned by rinsing them with distilled water and acetone using a hot ultrasonic cleaner device. Before making a deposition A digital film thickness meter (INFICON model SQM-160) was used to measure the deposition rate, which ranged from 0.5 to 2 Å/sec, while the vacuum chamber was evacuated to reach a base vacuum level of 2×10^{-4} mbar. Besides, Ag/MnS and Zn/MnS were annealed at a temperature 300 °C for 20 min. We examined

©2024 Sohag University

the films' crystallographic structure using a Philips X-ray diffraction (XRD) diffractometer (type PW1710, Netherlands). Ni was employed as the filter and Cu as the target material. The X-ray wavelength used was 1.541838 Å. The diffraction scan covered the range of 5° to 80° (2θ) to capture the diffracted X-ray patterns and analyze the crystal structure of the films. We used a field emission scanning electron microscope (FE-SEM) of the JSM-IT200 model to examine the surface shape of the films. The resolution of this instrument, equipped with Touch Scope TM functionality, was 3 nm (at 30 KV) and 4 nm (at 20 KV). The FE-SEM allowed for the examination of the film's surface at various magnifications ranging from 5 to 300,000X. During the imaging process, we maintained a low vacuum pressure of 10 to 100 Pa. Top of Form.

To examine the optical characteristics of the current films, a computer-programmable Jasco (V-570) UV/VIS/NIR spectrophotometer was utilized at room temperature. At normal incidence, the spectrophotometer's wavelength range was covered by 400 nm/min scan speed. This made it possible to calculate a number of optical constants, such as the dielectric constants (ε'), refractive index (n), extinction coefficient (k), optical band gap energy (E_g), and absorption coefficient (α). Using the two-probe approach, electrical properties were also studied, with measurements taking place at ambient temperature and up to 400°C. Also, we investigated the possibility of the annealed Zn pre-coating films and as-deposited MnS films on glass substrates as photo-catalysts for water purification, particularly for breaking down organic contaminants like methyl blue (MB) under Vis irradiation (lamp source 17 W). When the experiment first started, we tested the as-deposited MnS films and annealed Zn pre-coating films on glass substrates for their potential as photo-catalysts for water purification, specifically for degrading organic pollutants like methyl blue (MB). At the beginning of the experiment 100 ml of distilled water and 0.001 g of methylene blue were combined to create a solution. The pollutant's concentration as a result was 10 parts per million. After that, pour 20 mL of the mixture into a beaker. In the beaker: We immersed the films in a 0.001 g/mL methyl blue solution in the dark for one hour. We measured changes in absorption before and after exposing the films to visible light irradiation, taking measurements every five min for a total irradiation time of 120 min. A lamp emitting visible light was used for the visible light illumination. For gas sensor applications, we analyzed the optical absorption of the pure MnS films and Ag pre-coating films when exposed to I_2 gas. In addition, we conducted electrical testing on the films to detect CO_2 gas. We heated the films to a temperature of 300 °C and held them for a sufficient amount of time to stabilize the resistance value. After that, we passed a constant rate of CO_2 gas over the films to sense their properties.

3. Results and discussion

3.1. XRD diffraction and morphology

Fig. 1 shows that that the crystalline structure of the thin films in the 2θ range from 5º to 80º was ascertained by X-ray diffraction (XRD) analysis. According to the XRD data, every thin layer had an amorphous structure. Various factors, such as the deposition process, the composition of the films, or the presence of impurities or defects, contribute to this. The absence of clear diffraction peaks in the XRD pattern for amorphous thin films indicates that the atoms are not arranged coherently over a long distance.

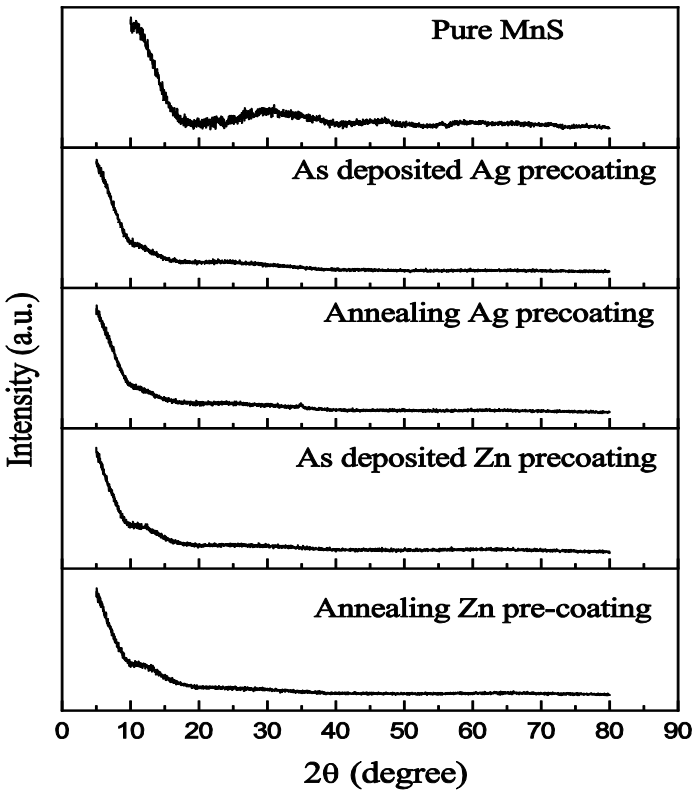

Figure 1: XRD diffraction analysis results for the samples.

A field emission scanning electron microscope (FE-SEM) was utilized to meticulously examine the surface characteristics of the MnS thin films, as well as those coated with Ag and Zn, as depicted in Fig. 2. The results of the analysis unveiled that the pure MnS film displayed impeccably smooth surfaces devoid of any voids or cracks, showcasing its amorphous nature. However, upon the addition of Ag or Zn as pre-coating layers, fascinating changes were observed. The films exhibited the presence of distinct grains, signifying the growth of nuclei on the surface. This suggests that the introduction of Ag or Zn triggered the formation of crystalline structures within the films. Further investigation of the Ag and Zn layers revealed intriguing variations. The particles in the Ag-coated film appeared to be larger in size compared to those in the Zn-coated film. This discrepancy can be attributed to the varying characteristics of Ag and Zn, which influenced the grain growth dynamics during the film deposition process. It's crucial to remember that the annealing of these films also played a significant role in influencing their surface morphology.

Upon annealing, we observed an interesting phenomenon. The particle size in both the Ag and Zn-coated films exhibited a noteworthy increase. Grain boundary migration caused the atoms within the films to rearrange themselves, leading to the migration and merging of particles with adjacent particles. This process resulted in the enlargement of the grains, ultimately altering the overall surface morphology of the films. Manganese (Mn) and Sulphur (S) were found in the pure MnS film by EDX analysis.

Manganese, Sulphur, and silver (Ag) were found in the Ag/MnS film. Similarly, the film with Cu pre-coating exhibited the presence of Mn, S, and Zn. Fig. 3 depicts the elemental proportions within the films.

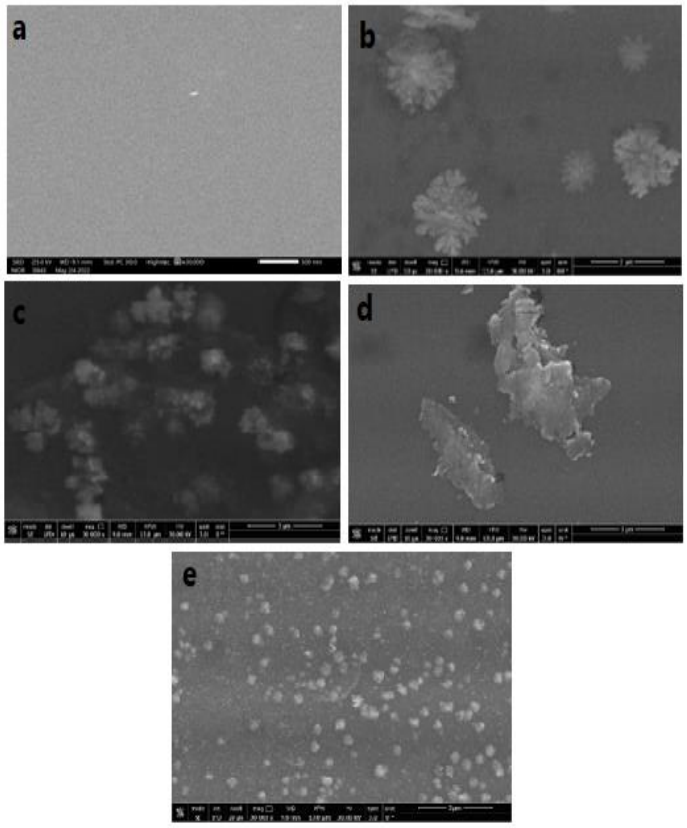

Figure 2: FE-SEM images for pure MnS (a), as deposited Ag pre-coated film (b), annealed Ag pre-coated film (c), as deposited Zn pre-coating (d) and annealed Zn Pre-coated (e).

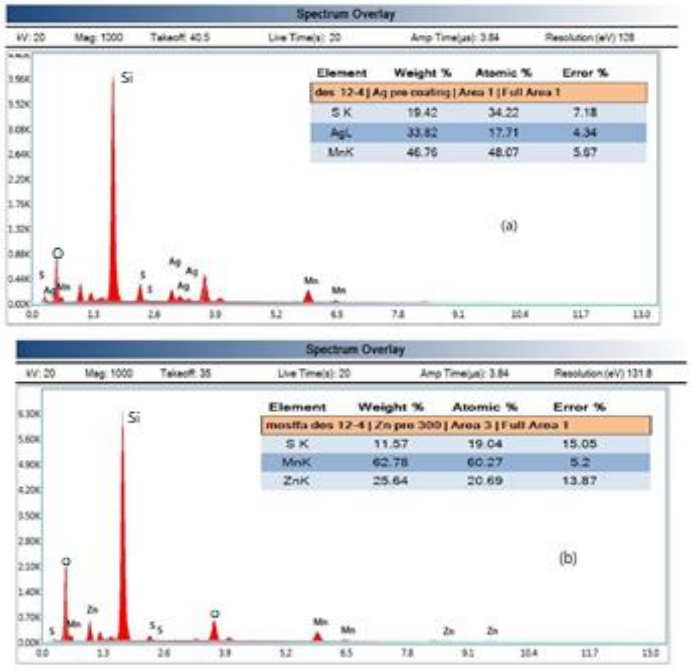

Figure 3: EDX image for as deposited Ag pre-coating (a) and, annealed Zn pre-coating films (b).

3.2. Optical characterization

The wavelength range in which the transmission and reflection were measured was 200–2500 nm at room temperature (Fig. 4). There was a red shift in the absorption of as-deposited (Ag and Zn) and annealed (Ag and Zn) pre-coating films compared to pure MnS, which means the energy gap values went down. Additionally, the average transmission of as-deposited Ag pre-coating decreased to 74% within the area that is visible, and after annealing at 300°C for 20 min, it further decreased to 69%. The reflection of as-deposited and annealed Ag pre-coating increased to 10%–30% within the area that is visible. Similarly, the transmission of as-deposited Zn pre-coating decreased to 37% in the visible region, but after annealing, it increased to 73%. The reflection of as deposited and annealed Zn pre-coating exchange increased from 8% to 45% in the visible region. A rise in the concentration of charge carriers as a result of the addition of silver and zinc can explain the observed changes in reflection and transmission in the visible and infrared regions. Furthermore, wavelength-dependent effects affected the amount of free carriers concentrated in the pre-coating layer in the near-infrared region. These effects could be attributed to the plasma oscillations of the free carriers [10–12].

As stated earlier, the first layer of metals being added causes a shift in the absorption edges towards lower gap energies. Changes in composition and annealing temperatures attribute to this shift. Additionally, the optical energy gap of the samples can be determined using Tauc's equation, as indicated by the following equations **[5], [13].**

$$(\alpha h\upsilon) = \beta(h\upsilon - E_g)^{1/r} \quad (1)$$

i.e $$ln(\alpha h\upsilon) = ln\,\beta + \frac{1}{r} ln(h\upsilon - E_g) \quad (2)$$

In the Tauc equation, the ratio of absorbance (Abs) to film thickness (d) is represented by α, while β is a constant independent of energy and $\frac{1}{r}$ is an exponent that determines the type of optical transition. To find $\frac{1}{r}$, we used the slopes of ln (αhν) versus ln (hν - E_g) plots, where due to absorption by bound electrons, there are abrupt decreases in transmission or sudden rises in absorbance in the visible and UV spectral bands. The fundamental absorption edge is the point at which absorption begins. The samples' band gap **[13]** determines the wavelength of the fundamental edges. For the pure MnS film, the as-deposited (Ag & Zn) pre-coating films, and the annealed (Ag & Zn) pre-coating films, we found that the value of $\frac{1}{r}$ was about 0.5. This means that direct transitions were possible. More accurate values of E_g can be obtained by further intercepts of $((\alpha h\upsilon)^{(1/n)} = 0$ on the hυ axis, as shown in Fig. 5. The energy gap values of 3.17, 2.57, 2.52, 2.6, and 1.9 eV were obtained for the pure MnS, as-deposited (Ag and Zn) pre-coating MnS and annealed (Ag and Zn) pre-coating MnS films, respectively.

In order to figure out how much structural disturbance there is in our films and what the localized states are near the optical energy gap (E), we need to know the Urbach energy (E_u) and the absorption coefficient (α). We can calculate the E_u using the equation [11]:

$$\alpha = \alpha_0 \exp\left(\frac{h\nu}{E_u}\right) \quad (3)$$

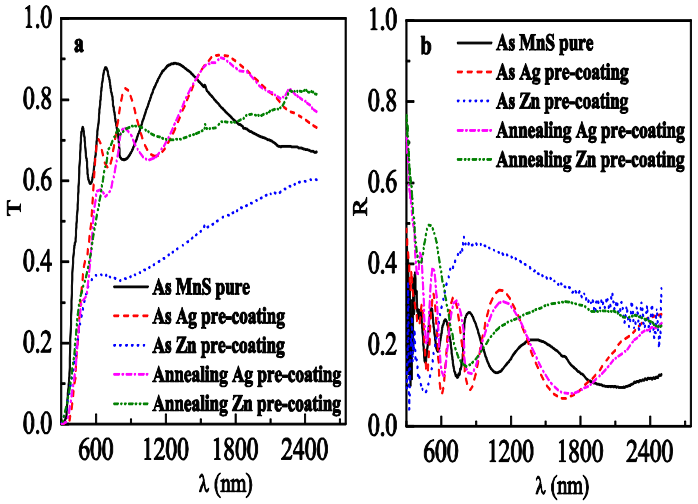

Figure 4: shows the transmission (a), and reflection (b) for as-deposited MnS, as deposited (Ag & Zn) pre-coating, and annealed (Ag &Zn) pre-coating.

Here, α_0 is a constant, and E_U represents the Urbach energy. The absorption coefficients at the UV and visible (VIS) ranges (α_{500}) for the current samples were measured, which fall in the range of 10^4-10^5. These values are highly significant for optoelectronic devices. In addition, the near-infrared (NIR) region exhibits values as low as $2x10^4$ cm^{-1}, indicating significant absorption and high transmission in those regions.

This implies that the present films contain relatively large levels of free carriers. Furthermore, by examining the slopes of the linear fitting of the plots of ln (α) vs (hυ), we were able to calculate the values of E_u (Fig. 6). For the MnS pure films, the E_u value is 0.307 eV, while for the as-deposited Ag pre-coating and Zn pre-coating films, the E_u values are 0.278 eV and 0.627 eV, respectively. After annealing, the E_u values for the Ag and Zn pre-coating films are 0.402 eV and 0.877 eV, respectively. These obtained values of E_u are almost lying in range of 0.299 – 0.571 eV for MnS [14, 15] and other amorphous semiconductors [16, 17]. Nevertheless, the relatively higher E_u value of 0.87 eV depicted for Zn/MnS film may be due to its tendency for rupturing of bonds and forming defects [18].

In many practical applications, it is important to know the refractive index (n) of a material. Additionally, studying the extinction coefficient (k) when exposed to a particular wavelength can help one understand the absorption characteristics of a medium. The following formulas can be used to estimate the refractive index (n) and extinction coefficient (k) [19], [20]:

$$n = \frac{(1+R)}{(1-R)} + \left[\left(\frac{1+R}{1-R}\right)^2 - (1+K^2)\right]^{\frac{1}{2}} \quad (4)$$

$$K = \frac{\alpha\lambda}{4\pi} \quad (5)$$

Here, R stands for reflection, α for absorption coefficient, and λ for incident light wavelength.

At a wavelength of 500 nm, Fig. 7A shows the refractive index values for pure MnS films that were deposited, films that were deposited with Ag and Zn pre-coating, and films that were annealed with Ag and Zn pre-coating. The refractive index values are 3.13, 2.37, 2.04, 3.3, and 5.7, respectively. Besides, all films have normal dispersion at different ranges between 1300 nm and 2500 nm. The observed differences in the refractive index at a fixed wavelength of 500 nm can be attributed to variou s factors, including optical basicity, ion coordination number, and material compactness. In addition, substantial absorption at energies greater than E_g may result in high refractive indices [21]. Which could be the reason for the high value (5.7) of the refractive index obtained for Zn/MnS having lower band gap energy of 1.9 eV.

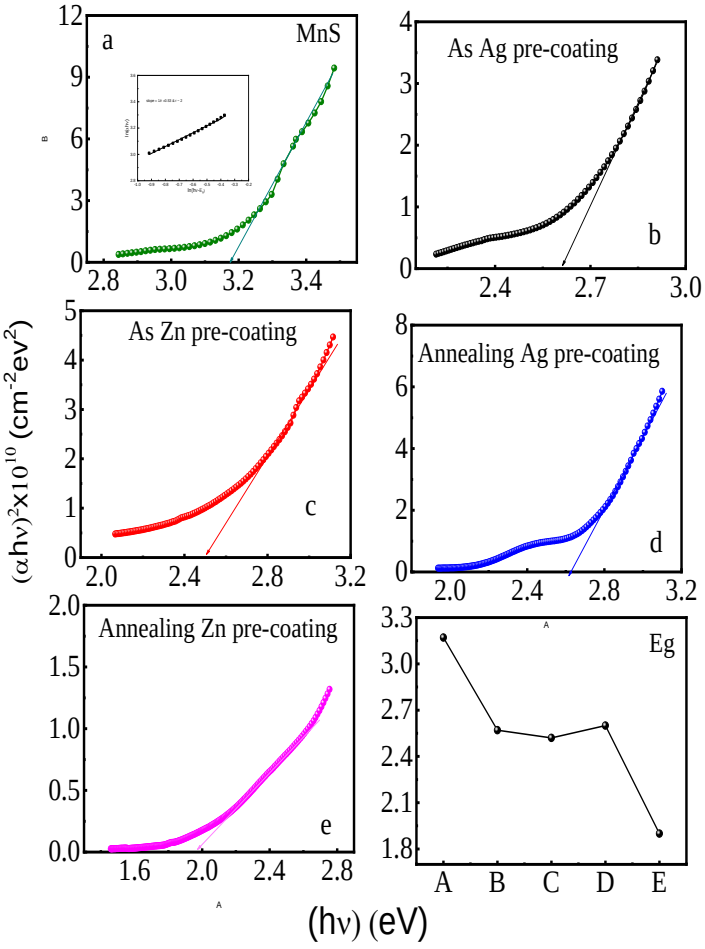

Figure 5: the optical band gap (E_g) values for as-deposited pure MnS (a), as-deposited (Ag & Zn) pre-coating (b) (c) and annealing (Ag & Zn) pre-coating (d) (e) films.

Moreover, the increase in the extinction coefficient in the infrared region indicates absorption resulting from free electrons or phonons (vibrational oscillations) within the samples (as seen in Fig. 7B). The real part of the dielectric constant provides information about the interaction between the crystal's photons and electrons. An increase in the real part of the dielectric constant indicates an improvement in the materials' optical response [22]. The dielectric constant is a crucial property that determines the interaction of materials with electromagnetic

radiation and their potential applications in optical devices and electronics. Furthermore, the analysis within the spectral variation of n (λ) and K (λ) revealed that the plots of ε' - λ^2 are linear in specific spectral ranges of λ. This linearity depends on the microstructural composition of the film, confirming the following relationship [23]:

$$\varepsilon' = n^2 - k^2 = \varepsilon_\infty - \frac{e^2}{\pi c^2}\frac{N}{m^*}\lambda^2 \quad (6)$$

$$\varepsilon' = \varepsilon_\infty + 4\pi x_c \quad (7)$$

$$\varepsilon' = \varepsilon_\infty - (\frac{\lambda}{\lambda_p}) \quad (8)$$

where N/m* is the ratio of the concentration of free carriers to the effective mass, and ε_L is the lattice's high-frequency dielectric constant. The plots' slopes and intercepts can be used to calculate the values of N/m*. Additionally, the plasma frequency ω_p can be determined using $\omega_p^2 = \frac{N}{m^*}\left(\frac{e^2}{\varepsilon_o \varepsilon_\infty}\right)$. All these parameters have been evaluated and listed in Table 1.

Table 1: Parameter values for optical dispersion and dielectric of pure MnS, as deposited (Ag and Zn) and annealed (Ag and Zn) films.

Components	N/m* (cm^{-3})	ϵ_∞	E_d (ev)	E_o (ev)	n_o	ϵ_L	ω_p (s^{-1}) x10^{14}
MnS	3.3x10^{34}	24	2.1	0.992	1.77	3.12	1.65
Ag pre-coating	4.5x10^{32}	14.4	16.95	4.73	2.14	4.58	4.7
Zn pre-coating	4.3x10^{34}	13.1	7.81	1.1	2.85	8.1	8.5
Annealing Ag pre-coating	1.7x10^{34}	4.77	0.828	0.95	1.37	1.87	1.6
Annealing Zn pre-coating	1.1x10^{34}	7.36	15.65	1.77	3.14	9.84	8.29

Understanding the dispersion of the index of refraction in our samples is crucial for ensuring accurate modeling and designing of devices [24]. Dispersion refers to the phenomenon where the index of refraction, denoted as n, can be determined within the low absorption region using the Wemple-Didomenico (WD) single oscillator model [25][26].

$$(n^2 - 1)^{-1} = -\frac{1}{E_o E_d}(h\upsilon)^2 + \frac{E_o}{E_d} \quad (9)$$

The calculation of the static refractive index, no, includes figuring out oscillator factors. E_o and E_d, as well as the energy of the photon E, and the dispersion energy E_d. These factors, along with the static refractive index, give insightful details regarding the structure. and density of the materials under study. Additionally, the lattice dielectric constant ε∞ can be determined by squaring no in accordance with the following equation:

$$n_o = \sqrt{1 + \frac{E_d}{E_o}} \quad (10)$$

3.3. Electrical properties

Investigating the electrical characteristics of metal sulfides has significant scientific and practical applications. Synthetic versions of sulfide metals, both pure and doped, hold potential for use in optical systems, photovoltaic, photodiodes, and magnetic recording systems [10], [24], [25], [27].

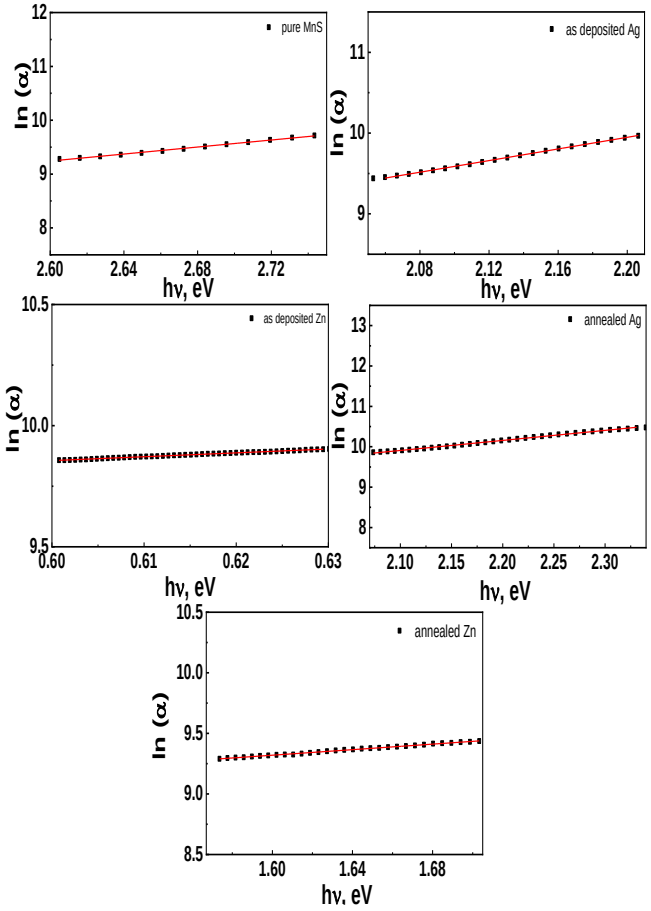

Figure 6: ln α vs hν plots for as-deposited MnS pure, as-deposited (Ag & Zn) pre-coating and annealed (Ag & Zn) pre-coating films.

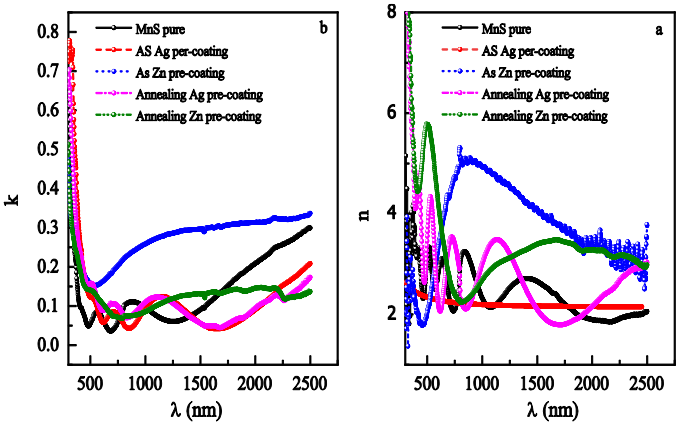

Figure 7: Displays the refractive index (a) and extinction coefficient (b) for as-deposited MnS, as-deposited (Ag & Zn) pre-coating and annealed (Ag & Zn) pre-coating films.

Using a two-probe technique, the resistances of pre-coated films (Ag and Zn) before and after annealing were examined within a temperature range of 30 to 400 °C. To calculate the

resistivity (ρ) of the samples, the following equation was employed:

$$\rho = \frac{RA}{l} \quad (11)$$

The resistivity (ρ) of the films was determined using the equation ρ = R (L/A), where R represents the measured resistance and A and L represent the area (thickness x width of the film) and length of the film, respectively. Fig. **8** illustrates that as the temperature increases, The films become less resistive., suggesting a semiconductor behavior in the samples.

The electrical conductivity of films at different temperatures, shown by how they react to heat, can be expressed mathematically for both films that have been as-deposited (Ag and Zn) and films that have been annealed (Ag and Zn) before they are coated. The relationship that captures this temperature dependence is as follows:

$$\sigma = \sigma_o e^{\frac{-\Delta E}{KT}} \quad (12)$$

i.e $$ln\sigma = ln\sigma_o - (\frac{\Delta E}{KT}) \quad (13)$$

and $$ln\ \sigma = ln\sigma_o - \frac{\Delta E}{1000K}\frac{1000}{T} \quad (14)$$

In the context of the provided equation, ΔE represents the activation energy, and σ_o signifies the pre-exponential factor. By analyzing the lnσ versus 1000/T (temperature) plots (refer to Fig. **9**), the slopes can be used to determine important information. Specifically, for as-deposited (Ag & Zn) pre-coating films, two activation energies can be observed: ΔE_1 for the extrinsic portion of the samples and ΔE_2 for the intrinsic portion. On the other hand, annealed (Ag & Zn) pre-coated films at 300°C exhibit single activation energy, ΔE_1, which can be calculated and documented in a corresponding table. The value of activation energy can be influenced by various factors, including temperature, pressure, and the presence of catalysts. Catalysts have the ability to lower the activation energy by offering an alternative pathway for the reaction that requires less energy. Understanding activation energy holds significance in numerous fields of chemistry, such as materials science, biochemistry, and environmental chemistry. Scientists can utilize this understanding to manipulate activation energies, enabling them to design chemical processes that are more efficient and effective while also developing new materials with desired properties.

3.4. Gas sensing test

In the gas sensing experiment, the optical properties of both as-deposited Ag pre-coating films and annealed Ag pre-coating films on glass substrates were tested. The main goal was to find out how I_2 exposure affected the optical absorption of MnS films that were deposited on these already-coated glass substrates. Fig. **10** illustrates the results of the experiment. It can be observed that, as the exposure time to I_2 gas increased, the fundamental absorption edge of the as-deposited Ag pre-coating films underwent a red shift towards higher wavelengths. This shift demonstrated that the gas was having an impact on the films. However, upon blocking the flow of gas, it was observed that the fundamental absorption edge blue-shifted, returning to its original position. Interestingly, the annealed Ag pre-coating films did not exhibit any sensitivity to I_2 gas, suggesting a different gas-sensing behavior compared to the as-deposited films. Besides, after heating the films to 200 degrees Celsius and holding them there long enough to stabilize the resistance value, the films were electrically tested to detect Co2 gas. After that, the gas was pushed through the films at a steady rate. As shown in Fig. **11.**

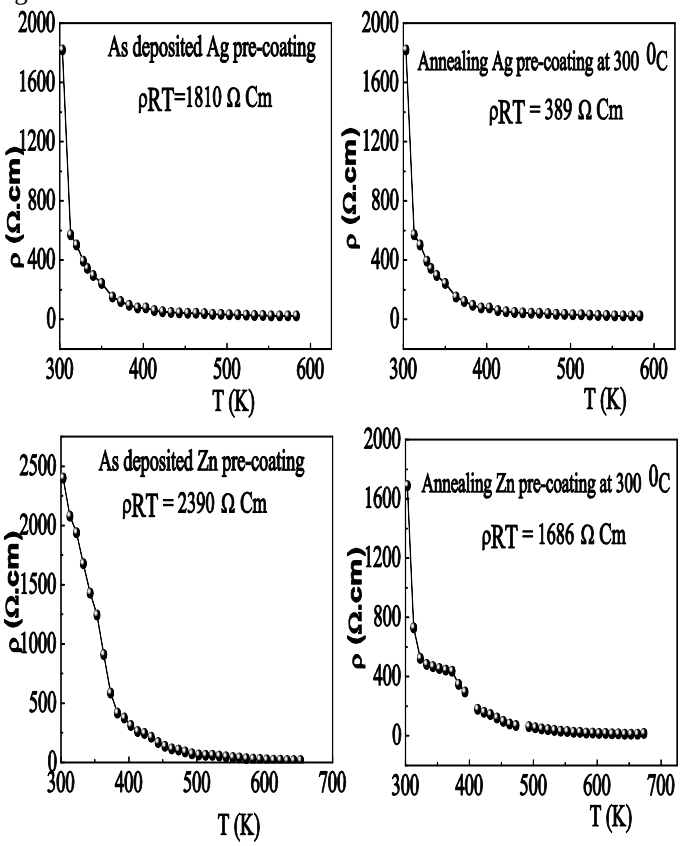

Figure 8: The resistivity (ρ) for as-deposited (Ag & Zn) pre-coating and annealed (Ag & Zn) pre-coating films.

The resistance is constant for a period then after passed Co_2 gas for as deposited Ag pre-coting pure as the length of the gas passage expands, the resistance rises; when the gas passage is stopped, the resistance falls to its initial position. While annealing Ag pre-coating films are not sensing to Co_2 gas. Additionally, the films were subjected to electrical testing to assess their gas sensing capabilities towards Co_2 gas. The testing procedure involved raising the temperature of the films to 200°C and allowing them to stabilize to obtain a consistent resistance value. Subsequently, the Co_2 gas was passed through the film at a constant flow rate. Fig. **11** presents the results derived from this experiment. It can be observed that initially, the resistance remains constant for a certain period. However, upon the introduction of CO_2 gas for the as-deposited Ag pre-coating films, the resistance starts increasing as the gas passage time continues. Once the gas flow is stopped, the resistance gradually decreases, eventually returning to its original position. In contrast, the annealed Ag pre-coating films did not exhibit any response or sensitivity towards CO_2 gas, suggesting they are not effective in sensing this particular gas.

3.5. Organic pollutant decomposition:

An annealing Zn pre-coating film, which has an energy band gap (E_g) of 1.9 eV were added to 20 ml MB solution in a beaker then it was left in darkness for an hour to ensure that all reactions had ceased. After the dark incubation period, the beaker containing

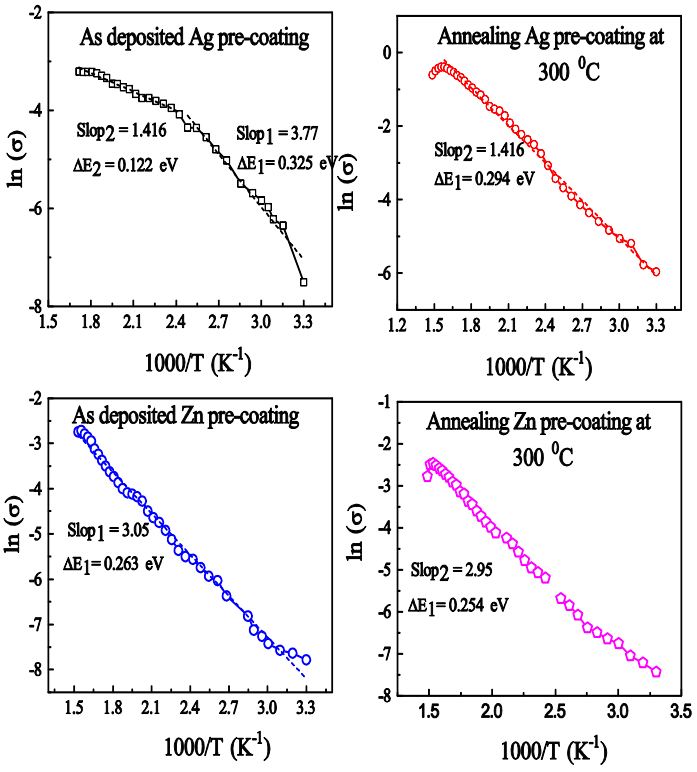

Figure 9: Depicts the graphical representation of the relationship between ln (σ) and 1000/T for both as-deposited (Ag & Zn) pre-coating films and annealed (Ag & Zn) pre-coating films.

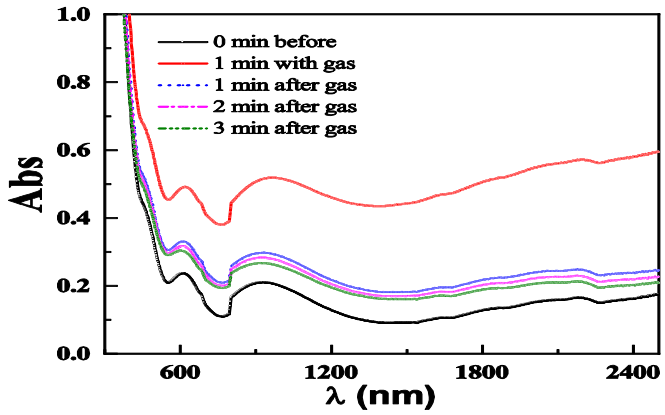

Figure 10: Shows the absorption of the film before and after exposure to gas as a function of wavelength specifically for the as-deposited Ag pre-coating films.

the solution and the Zn pre-coating film was exposed to visible light irradiation for specific time intervals. The photocatalysis properties of the Zn pre-coating film, coupled with visible light, allow organic contaminants to oxidize and transform into non-toxic compounds like water and CO_2. Under the influence of excitation energy exceeding the band gap of the annealing Zn pre-coating catalyst, the conduction band (C_B) is stimulated to attract electrons from the valence band (V_B). In the valence band, holes (h^+) are produced concurrently. The hydroxyl ions (OH^-) and superoxide anion (O^{2-}) can be produced by the photo-generated electrons (e^-). from molecular oxygen (O_2) [28]. Moreover, the hole (h^+) can directly oxidize organic materials, resulting in the formation of reactive intermediates. Alternatively, it can react with water (H_2O) to generate hydroxyl radicals (OH) [29]. The pronounced oxidative capabilities of O^{2-} and OH^- enable the complete degradation of various inorganic compounds and the oxidation of the majority of methylene blue (MB) into CO_2 and water [30]. To evaluate the photocatalysis activity of the annealing Zn pre-coating films, we assessed the photo-degradation of the MB dye. The distinctive absorption peak of MB was chosen as the observed parameter for the degradation process of photocatalysis at 664 nm [31]. Using MB as an organic model, Fig. 12 shows the photocatalysis degradation activity of both pure MnS and the annealing Zn pre-coating catalyst. The findings unequivocally show that as exposure times grow, the degradation ratio of MB progressively rises. Within 140 min of exposure, the degradation ratio reaches 41% for pure MnS, while the annealing Zn pre-coating achieves an 81.5% degradation ratio within 120 min.

Fig. 13 shows the efficiency of dissociation of the pollutant and degradation (D), according to the following relations [3]:

$$\eta = \frac{A_o - A}{A_o} \times 100 \quad (15)$$

$$D = \ln\left(\frac{A}{A_o}\right) \quad (16)$$

$$t_{\frac{1}{2}} = \left(\frac{\ln(2)}{k}\right) \quad (17)$$

In the experimental setup, the values A_o and A represent the peak's vertex in the first and second measurements, respectively. These values serve as indicators of the initial and subsequent concentrations of the organic pollutant under investigation. Meanwhile, the variable k corresponds to the degradation rate constant, which characterizes the speed at which the organic pollutant breaks down. Additionally, the parameter $t_{1/2}$ denotes the half-life of the organic pollutant, which represents the time required for half of the initial concentration to disintegrate. For MnS the values of $t_{1/2}$ is 246 min and γ is $28.2 \times 10^{-4} min^{-1}$ while annealed Zn pre-coating values of $t_{1/2}$ is 52 min and γ is 0.0134 min^{-1}.

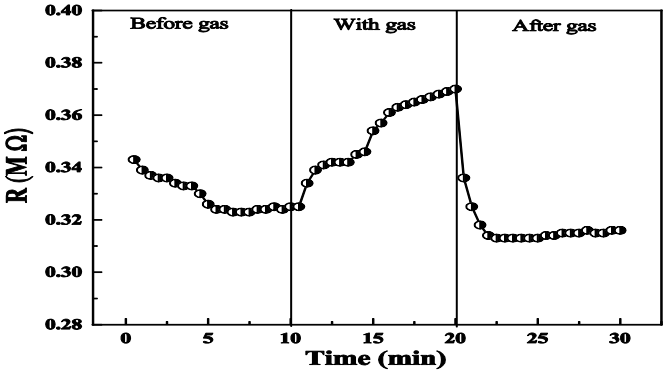

Figure 11: Depicts the resistance of the film before and after exposure to gas as a function of time specifically for the as-deposited Ag pre-coating films.

4. Conclusion

In summary, the thermal evaporation process was successfully used to prepare manganese sulfide and metals as pre-coating layer films. Analysis using X-ray diffraction revealed that every thin layer had an amorphous structure, indicating the lack of long-range order in the arrangement of atoms. The FE- SEM results revealed smooth surfaces without voids or cracks for all the samples, and the addition of Ag or Zn as pre-coating layers resulted in the presence of grains. The existence of Mn and S in the pure MnS film was verified by EDX analysis. The absorbance, transmission, and reflection measurements indicated changes in the energy gap values and charge carrier concentration due to the addition of Ag and Zn. Tauc equation and analysis of absorption coefficient provided energy gap values for the different films. The Urbach energy values indicated the level of structural disturbance and localized states near the energy gap. Dispersion of the index of refraction was determined using the Wemple-DiDomenico single oscillator model. Semiconductor behavior was evident in the films' electrical properties. Gas sensing studies were used to show how I_2 and Co_2 gas affected the optical absorption of the Ag/MnS films as they were being deposited. The response and recovery times for I_2 and Co_2 were found to be 1 min, 3 min, and 0.97 min and 1.9 min, respectively. In addition, annealed Zn/MnS exhibited an efficiency of roughly 81.5%, a γ of 0.0134 min^{-1}, and a $t_{1/2}$ of 52 min.

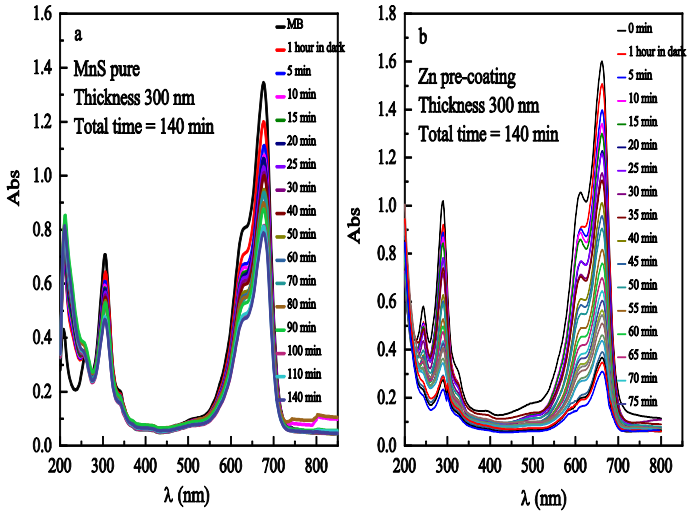

Figure 12: Photocatalysis for MnS pure (A) and for the as-deposited Zn pre-coating films (B).

CRediT authorship contribution statement:

E. Kh. Shokr; visualization, supervision, conceptualization, resources, review and editing, **H. M. Ali**; Conceptualization, validation, writing-review and visualization, **H. A. Mohamed**; validation, and review, **M. F. Hasaneen**; validation, writing-review and **A. A. Ismail**; software, formal analysis, investigation, data curation, methodology, writing (original draft preparation and editing).

Data availability statement

The data used to support the findings of this study are available from the corresponding author upon request.

Declaration of competing interest

The authors declare that they have no known competing financial interests or personal relationships that could have appeared to influence the work reported in this paper.

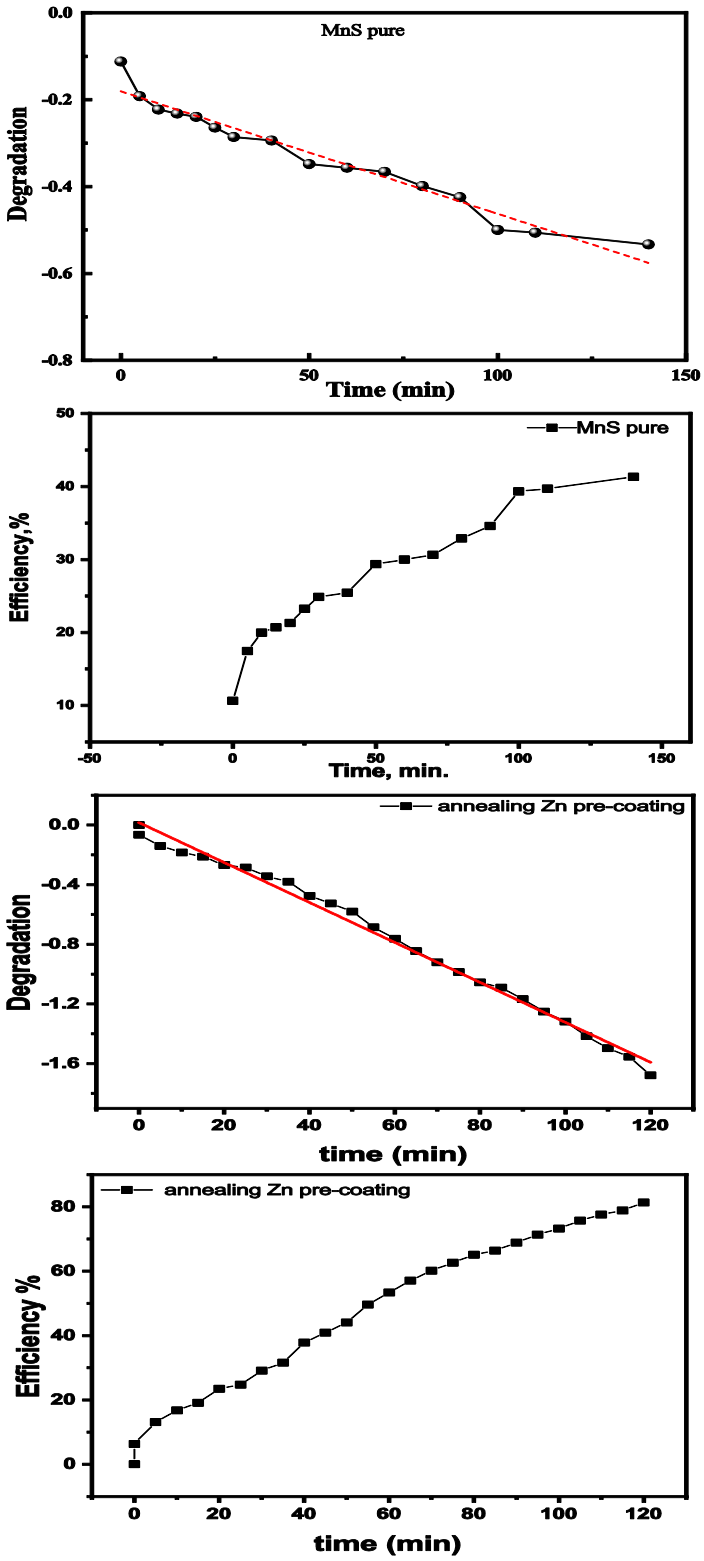

Figure 13: Degradation and efficiency for Pure MnS and for the as-deposited Zn pre-coating films.

References

[1] S. Khan, W. Lei, K. Takagi, A. Uchida, and N. Suzuki, *materials latters*, 300 (2021) 3–6.

[2] T. Liu, Y. Li, J. Yin, J. Li, and H. Wu, *Physica E*, 116 (2020) 113711.

[3] A. Fakhri and D. S. Kahi, *Journal of Photochemistry & Photobiology, B: Biology*, 22 (2011) 265504.

[4] C. Chang, M. Teng, J. Chen, Y. Lin, and C. Chen, *Appl. Surf. Sci*, 558 (2021) 149875.

[5] A. Hannachi, A. Segura, and H. Maghraoui-meherzi, *Mater. Chem. Phys*, (2016) 1-7.

[6] M. Girish, R. Sivakumar, C. Sanjeeviraja, and Y. Kuroki, *Opt. - Int. J. Light Electron Opt*,126 (2015) 2074-2079.

[7] C. Ulutas, E. Guneri, F. Kirmizigul, G. Altindemir, F. Gode, and C. Gumus, *Mater. Chem. Phys*, 138 (2013) 817–822.

[8] C. Gu, C. Ulutas, and Y. Ufuktepe, *Optical Materials*, 29 (2007) 1183–1187.

[9] T. Veeramanikandasamy, K. Rajendran, K. Sambath, and P. Rameshbabu, *Mater. Chem. Phys*, 171 (2016) 328–335.

[10] E Kh Shokr, *Semicond. Sci. Technol*, 15 (2000) 247–253.

[11] M. F. Hasaneen, H. M. Ali, M. M. A. El-raheem, and A. M. A. Hakeem, *Mater. Sci. Eng. B*, 262 (2020) 114704.

[12] E. Shanthi, V. Dutta, A. Banerjee, and K. L. Chopra, *journal of applied physics*, 6243 (2014) 1980.

[13] Optical properties of solid, mark fox, Oxford university press, United States, 2001.

[14] Z. Amara, M. Khadraoui, R. Miloua, A. Boukhachem, A. Ziouche, A. Nakrela, A. Bouzidi, *physica-b-condensed-matter*, 585 (2020) 412121.

[15] M. Girish, T. Dhandayuthapani, R. Sivakumar, C. Sanjeeviraja, *J. Mater. Sci: Mater. Electron*, 26 (2015) 3670–3684.

[16] Susheel Arora, Virender Kundu, D. R. Goyal, and A. S. Maan, *International Scholarly Research Network*, 2012 (2012).

[17] Susheel Arora, Virender Kundu, D. R. Goyal, and A. S. Maan, *International Scholarly Research Network*, 2012 (2012).

[18] G. Senthil Murugan, Yasutake Ohishi, *Journal of Non-Crystalline Solids*, 341 (2004) 86–92.

[19] A. Ashery, A. A. M. Farag, and M. A. Shenashen, *Synth. Met*, 162 (2012) 1357–1363.

[20] E. KH. Shokr, *Journal of Physics and Chemistry of Solids*, 53 (1992) 1215–1219.

[21] Aspnes, David E., and A. A. Studna, *Physical review B*, 27 (1983): 985.

[22] M.A. Hadi, N. Kelaidis, P.P. Filippatos, S.-R.G. Christopoulos, A. Chroneos, S.H. Naqib, A.K.M.A. Islam, *journal of materials research and technology*, 18 (2022) 2470 -2479.

[23] E. K. Shokr, M. M. Wakkad, H. A. A. El-ghanny, and H. M. Ali, *Journal of Physics and Chemistry of Solids*, 61 (2000) 75–85.

[24] M. F. Hasaneen, Y. A. T. H. M. Ali, and M. R. Ahmed, *Appl. Phys A*, (2020) 1–13.

[25] S. H. Wemple and M. DiDomenico, Jr, *physical review B*, 3 (1971) 1338–1351.

[26] G. R. Behavior, *international conference on optical storage*, 7 (1973) 8.

[27] M. Dhanam, K. Arts, and K. Balakrishnan, *Journal of Ovonic Research*, 6 (2010) 1-11.

[28] et al K. Liu, Z.R. Shen, Y. Li, *Sci. Rep*, 4 (2014) 6023.

[29] M. F. H.R. Rajabi, *Mater. Sci. Semicond. Process*, 31 (2015) 478–486.

[30] D. A. T. A. Fujishima, T.N. Rao, *J. Photochem. Photobiol. C Photochem. Rev*, 1 (2000) 1–21.

[31] T. M. N. Shimizu, C. Ogino, M.F. Dadjour, *Ultrason. Sonochem*, 14 (2007) 184–190.